Observational Evidence of Large-Scale Multiple Reconnection at the Earth's Dayside Magnetopause

S. A. Fuselier, S. M. Petrinec, K. J. Trattner, J. M. Broll, J. L. Burch, B. L. Giles, R. J. Strangeway, C. T. Russell, B. Lavraud, M. Øieroset, et al.

HAL Id: insu-03678171
https://insu.hal.science/insu-03678171

Submitted on 25 May 2022

Observational Evidence of Large-Scale Multiple Reconnection at the Earth's Dayside Magnetopause

RESEARCH ARTICLE

Key Points:
- Multiple reconnection X lines are observed at the Earth's magnetopause
- Their particle signatures indicate that the X lines are quasi-stationary and far apart from one another

Correspondence to:
S. A. Fuselier,
sfuselier@swri.edu

S. A. Fuselier[1,2], S. M. Petrinec[3], K. J. Trattner[4], J. M. Broll[1,2], J. L. Burch[1], B. L. Giles[5], R. J. Strangeway[6], C. T. Russell[6], B. Lavraud[7], M. Øieroset[8], R. B. Torbert[9], C. J. Farrugia[9], S. K. Vines[10], R. G. Gomez[1], J. Mukherjee[1], and P. A. Cassak[11]

[1]Southwest Research Institute, San Antonio, TX, USA, [2]Department of Physics and Astronomy, University of Texas at San Antonio, San Antonio, TX, USA, [3]Lockheed Martin Advanced Technology Center, Palo Alto, CA, USA, [4]Laboratory for Atmospheric and Space Physics, University of Colorado Boulder, Boulder, CO, USA, [5]Goddard Space Flight Center, Greenbelt, MD, USA, [6]University of California, Los Angeles, CA, USA, [7]Institut de Recherche en Astrophysique et Planétologie, Université de Toulouse, CNRS, UPS, CNES, Toulouse, France, [8]Space Sciences Laboratory, University of California, Berkeley, CA, USA, [9]University of New Hampshire, Durham, NH, USA, [10]Applied Physics Laboratory, Laurel, MD, USA, [11]West Virginia University, Morgantown, WV, USA

Abstract Magnetic flux ropes of various scale sizes have been observed at the Earth's magnetopause for four decades. These multiple structures resulting from reconnection have complex internal field and plasma signatures, and evolve as they propagate along the dayside magnetopause. Here plasma and magnetic field observations from the Magnetospheric Multiscale (MMS) mission are used to describe a different type of large-scale multiple reconnection, magnetic flux rope-like structure at the Earth's magnetopause. These observations show at least two X lines separated by many Earth radii. Unlike smaller-scale flux ropes or flux transfer events, these multiple X lines are stationary and consist of primary and secondary X lines. The secondary X line is either transient in time or does not reconnect all of the magnetic flux that reconnects at the primary X line. Several examples of these large-scale reconnection structures are tabulated. These examples indicate that this type of structure may be common at the magnetopause at least for a narrow range of interplanetary magnetic field clock angles.

Plain Language Summary Magnetic reconnection at the Earth's magnetopause is the driver for the interaction between the solar wind and Earth, that is, space weather. This reconnection is usually considered to occur along a long reconnection X line across the magnetopause. However, the observations here show that there are multiple X lines at the magnetopause where reconnection is occurring. These X lines do not appear to move and there appears to be a primary X line and at least one secondary X line.

1. Evidence of Multiple Reconnection at the Earth's Magnetopause

Magnetic reconnection occurs at the Earth's magnetopause at low latitudes when the interplanetary magnetic field (IMF) has a southward ($-B_z$) component. Under these conditions, reconnection occurs between magnetosheath and magnetospheric magnetic field lines that are either nearly oppositely directed (antiparallel reconnection) or at an oblique angle to one another (component reconnection). The empirically derived maximum magnetic shear model (Trattner et al., 2007) unifies these two types of reconnection. This model was developed from over 130 cusp crossings (using more than 3,000 individual measurements in the cusp). In this model, for certain IMF conditions, reconnection occurs along an extended, continuous X line that stretches across the entire dayside magnetopause from dawn to dusk. For example, if IMF B_y is appreciable, for example, $|\pm B_y| \sim |-B_z|$, (the $\pm$ sign indicates that B_y can have any sign, but the – sign indicates that B_z is negative) then antiparallel reconnection occurs on the flanks of the magnetopause and component reconnection occurs along an extended X line. This component X line cuts across the noon-midnight meridian and connects the two antiparallel reconnection X lines on the flanks. The location and orientation of the component X line relative to the subsolar point depends on season and the strength and sign of the IMF B_y component. There have been several tests of this empirical model using in situ and remote sensing observations at the magnetopause (Dunlop et al., 2011; Fuselier et al., 2011; Petrinec et al., 2011, 2016; Trattner et al., 2012, 2017).

Although there is evidence that a single long, continuous reconnection X lines at the dayside magnetopause can occur (e.g., Fuselier et al., 2002; Phan et al., 2000; Trattner et al., 2007), there is also evidence that multiple

reconnection X lines at the dayside boundary are common (e.g., Vines, Fuselier, Petrinec, et al., 2017). These multiple X lines have a wide range of scale sizes. At small scales, simulations predict the formation of ~100 km "islands" separated by X lines on either side (e.g., Drake, Swisdak, Schoeffler, et al., 2006). Three-dimensional simulations show that reconnection with a guide field produces helical magnetic structures (i.e., flux ropes; Daughton et al., 2011; Nakamura et al., 2016). While these islands may play an important role in plasma energization (e.g., Drake, Swisdak, Che, et al., 2006), they appear to be confined to near the reconnection diffusion region (e.g., Eastwood et al., 2016).

At intermediate scales, there are two (or more) X lines parallel to one another and separated by ~1 Earth radius (R_E). Often, the region between the X lines has very complex structure (e.g., Kacem et al., 2018; Øieroset et al., 2016). The 1 R_E scale size of these structures suggests that they could be a form of flux transfer events (FTEs) or, in three dimensions, flux ropes at the magnetopause (e.g., Lee & Fu, 1986). However, there are other interpretations of FTE magnetic topologies that do not require multiple X lines (e.g., Owen et al., 2008; Russell & Elphic, 1978; Scholer, 1988; Southwood et al., 1988).

At larger scales, probably the largest scale possible at the magnetopause, there is evidence of multiple reconnection X lines that may be separated by many R_E (e.g., Fuselier et al., 2011; Hasegawa et al., 2010; Trattner et al., 2012). The region between the X lines could encompass a large portion of the dayside magnetopause. Global simulations of the magnetopause also show X lines separated by very large distances (e.g., Chen et al., 2017; Hoilijoki et al., 2017; Raeder, 2006). In these recent simulations, the X lines move along the magnetopause, but not necessarily in one direction or at a constant speed (Hoilijoki et al., 2017). However, in these simulations, X lines can move at speeds from one to several hundreds of kilometers per second along the magnetopause in one direction for several minutes (e.g., Hoilijoki et al., 2017; Raeder, 2006). Observations of multiple X lines at these largest scales for southward IMF conditions are the subject of this paper.

In this paper, observations from the MMS spacecraft at a crossing of the subsolar magnetopause are used to demonstrate that there are at least two X lines at the magnetopause and that the X lines are far apart from one another. One X line is located several R_E from the spacecraft, probably at the location predicted by the maximum shear model. A second X line is located near the spacecraft. Both X lines are quasi-stationary, a feature that sets these observations apart from previous observations and simulations of multiple X lines at the magnetopause. Section 2 describes the MMS instrumentation and how it is used to determine field topologies, directions, and distances to the X lines. Section 3 describes the observations for the example magnetopause crossing. Section 4 discusses the observations and lists several other magnetopause crossings with similar characteristics. These other events suggest that multiple X line structures of this type are not uncommon at least for a fairly narrow range of IMF clock angles.

2. MMS Mission, Instrumentation, Data Products, and Their Use

The MMS mission was designed to use the near-Earth environment as a plasma laboratory to investigate magnetic reconnection (Burch et al., 2016). The spacecraft orbits maximized encounters with reconnection diffusion regions at the low-latitude dayside magnetopause during the prime mission (Fuselier et al., 2016). In particular, the orbits passed through the subsolar point, where reconnection signatures are common, especially for southward IMF. Magnetopause crossings at or near the subsolar magnetopause have a unique property. The magnitudes of the draped magnetosheath and magnetospheric magnetic fields have local maxima at this location. Ions propagating from a distant reconnection site must conserve their first adiabatic invariant as they propagate into a region where the magnetic field magnitude is larger. This conservation results in specific characteristics in the ion populations and these characteristics are used here to determine the distances to the reconnection X lines (Broll et al., 2017; Fuselier et al., 2014).

Electron observations in this paper are from the Fast Plasma Investigation (Pollock et al., 2016). The Dual-Electron Spectrometers measure full 3-D electron distributions from 10 eV to 30 keV in as little as 7 ms. Much lower time resolution measurements (4.5-s resolution) are used here to help identify the plasma regions. In addition, the electron fluxes parallel and antiparallel to the field are used to identify magnetic field topology and the direction(s) to reconnection X line(s). Electron fluxes have been used extensively in this manner (Fuselier et al., 1995, 1997, 2011, 2012, 2014; Lavraud et al., 2005, 2006; Russell et al., 2017; Vines, Fuselier, Petrinec, et al., 2017).
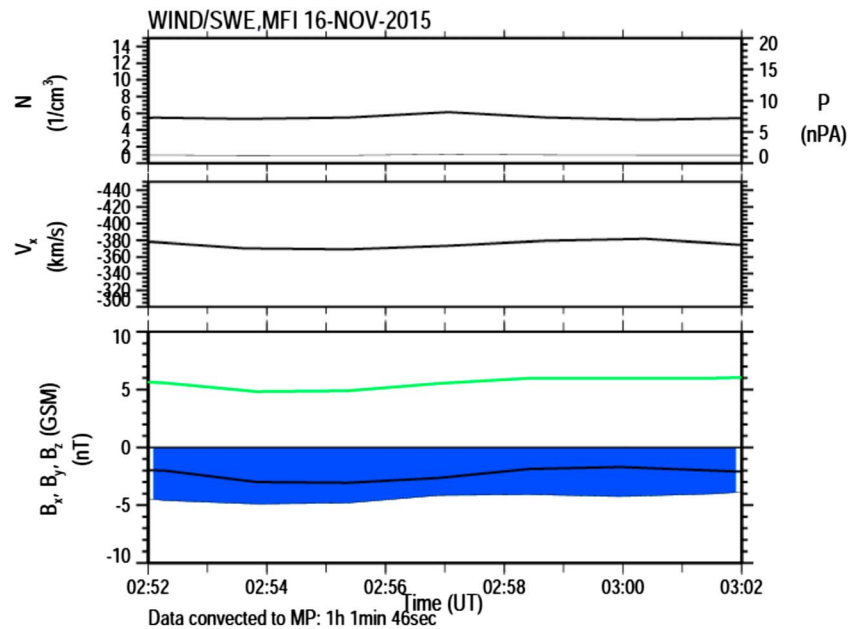
Figure 1. Solar wind for the MMS magnetopause crossing on 16 November 2015. The solar wind density and velocity were relatively steady for the crossing. The magnetic field was southward (B_z, negative; blue shaded region to emphasize that it was southward through the interval), had a strong, positive B_y component (green line), and a relatively small, negative B_x component (black line).

Ion observations in this paper are from the Hot Plasma Composition Analyzer (HPCA; Young et al., 2014). This ion mass spectrometer measures full 3-D distributions of five major ion species from 1 eV to 40 keV in 10 s. The 3-D proton distributions are used in conjunction with the electron measurements to determine the direction(s) to X line(s). In addition, characteristics of the various ion populations are used to determine the distance(s) to X line(s).

Magnetic field measurements in this paper are from the MMS FGM magnetometers (Russell et al., 2016). The magnetic field measurements are used to identify the magnetopause current layer. They are also used to determine the parallel and antiparallel directions for the electron measurements and to determine pitch angle for the 3-D proton distributions.

The solar wind conditions for the events in this paper are from the WIND spacecraft. The IMF (Lepping et al., 1995) is used in the maximum magnetic shear model to predict the location of the reconnection X line. The solar wind velocity (Ogilvie et al., 1995) is used to convect the IMF to the magnetopause.

3. Observations on 16 November 2015

On 16 November 2015 at 0256–0258 UT, the MMS spacecraft crossed the subsolar magnetopause from the magnetosphere to the magnetosheath. The solar wind conditions for this crossing, from the WIND spacecraft and convected to the magnetopause with a convection time of ~61 min, are shown in Figure 1. The density and solar wind velocity were relatively constant over the 10-min interval. The IMF was southward and steady, with $+B_y \sim |-B_z|$ and a relatively small $|-B_x|$ for the interval and for several minutes on either side of the interval (not shown). For northern hemisphere winter and these IMF conditions, the maximum magnetic shear model (Trattner et al., 2007) predicts a component reconnection line stretching across the dayside magnetopause, crossing the noon meridian at mid northern latitude. The MMS spacecraft are well south of this component reconnection line. Thus, for the solar wind conditions in Figure 1, the MMS spacecraft crossed the subsolar magnetopause several R_E south of a predicted component reconnection X line.

Figure 2 shows 20 min of MMS1 HPCA and FGM data. Panels from top to bottom (Figures 2a–2f) are the omnidirectional proton flux, the proton bulk flow velocity components in GSM coordinates, the magnetic field components in GSM coordinates, and the total magnetic field. The spacecraft is in the low-latitude
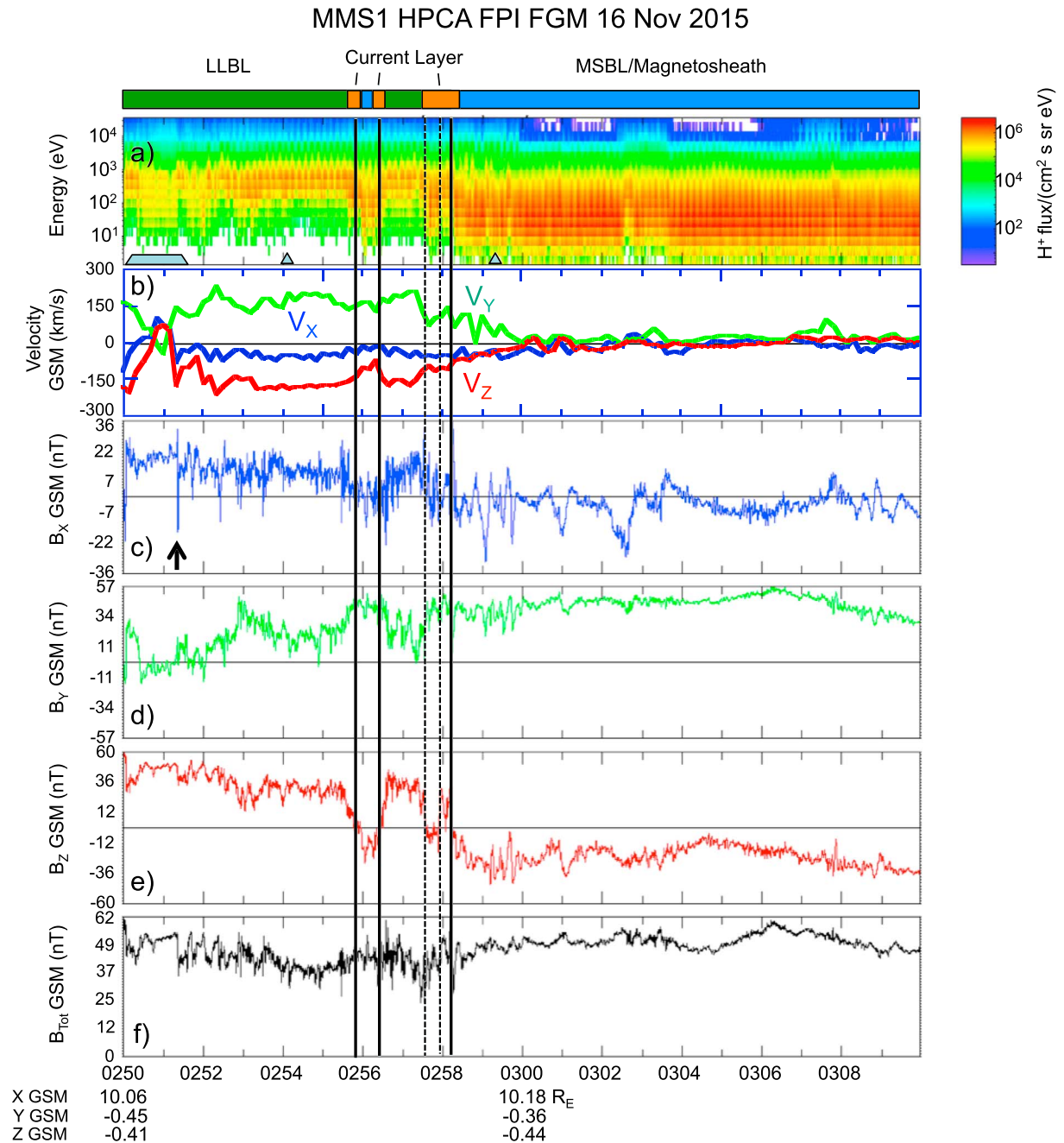
Figure 2. (a–f) The omnidirectional proton flux, the proton bulk flow velocity components, the three components of the magnetic field, and the total magnetic field for the magnetopause crossing very near the subsolar point on 16 November 2015. The spacecraft was in the LLBL at the beginning of the interval. In the LLBL, the flow velocities were generally higher than in the magnetosheath. It crossed the magnetopause several times and ended in the magnetosheath at the end of the interval. The MSBL and magnetosheath proper are distinguished by the presence and absence of energetic protons above 10 keV, respectively. In the LLBL, B_z (e) was dominant, but there was often a substantial B_y component (d). There are some positive/negative excursions in the B_x component (c) that may be FTE-like signatures. However, the long period from 0250 to 0251:30 UT (gray trapezoid in (a)) was characterized by relatively stable magnetic field direction and magnitude. The gray triangles in (a) identify the two distributions in Figure 5.

boundary layer (LLBL) at the start of the interval. The LLBL is defined here and elsewhere as the layer of reconnected magnetic field lines earthward of, but adjacent to, the magnetopause. The reconnected field line could be open (connected to a single X line) or closed (connected to two X lines in opposite directions along the field). The spacecraft makes several complete and partial crossings of the

magnetopause current layer between 0256 and 0258:15 UT. After these crossings, the spacecraft is in the magnetosheath and magnetosheath boundary layer (MSBL) for the rest of the interval. The MSBL is defined here as elsewhere (e.g., Cowley, 1982) as the layer of reconnected magnetosheath field lines sunward of, but adjacent to the magnetopause. Similar to the LLBL, the field lines in the MSBL can be open or closed.

The proton fluxes (Figure 2a) in the LLBL are generally lower than those in the magnetosheath, especially at energies between about 10 and 100 eV. At energies above 10 keV, the fluxes in the LLBL are generally higher than those in the magnetosheath. The fluxes above 10 keV provide a means for distinguishing between the magnetosheath "proper" and the MSBL. In the magnetosheath proper (hereafter simply the magnetosheath), the fluxes above 10 keV are nearly at background (for example from 0304 to 0306 UT) while the fluxes above 10 keV in the MSBL are less than, but comparable to those in the LLBL. Magnetic field lines in the MSBL thread the magnetopause current layer, allowing energetic magnetospheric ions to escape from the LLBL. In addition, there is a population of magnetosheath ions that are reflected off the magnetopause in the MSBL, and this population has higher energy than the ion population in the magnetosheath proper (e.g., Cowley, 1982; Fuselier et al., 1991; Vines et al., 2015; Vines, Fuselier, Trattner, et al., 2017). Thus, the presence of an MSBL with >10-keV protons is one piece of evidence of reconnection at the magnetopause. The flow velocities (Figure 2b) are generally very high in the LLBL and near zero in the magnetosheath. The high bulk velocities in the LLBL are indicative of reconnection at the magnetopause. The near-zero velocities in the magnetosheath are consistent with the spacecraft location in the subsolar region. The bulk flow velocities from 0250 to 0251:50 UT in the LLBL are lower and in a different direction than the rest of the LLBL. As discussed below, the reason for these lower velocities is the presence of multiple proton populations with different velocities along the field.

At the subsolar point, the magnetospheric magnetic field should be $|B| \sim | + B_z|$ in the absence of reconnection. There are certainly times when the B_z component of the magnetic field (Figure 2e) is dominant, for example, near 0251 UT. However, for most of the LLBL interval in Figure 2, the B_y component (Figure 2d) in the LLBL is similar to that in the magnetosheath. This similarity is another consequence of magnetic reconnection. The open magnetopause is a rotational discontinuity and the B_y field must rotate from the magnetosheath orientation to the magnetospheric orientation through the discontinuity. Therefore, B_y should be positive in the LLBL. Empirical models also impose a finite B_y at the magnetopause using a parameter that specifies the amount of "diffusion" of the magnetosheath field into the magnetosphere (see Tsyganenko, 2014). The B_x component of the magnetic field (Figure 2c) is nearly aligned with the magnetopause normal vector at the subsolar point. Thus, this component is expected and observed to be small at the magnetopause. Of particular interest are sharp bipolar signatures in the B_x component near the magnetopause because these excursions in the normal component are an indication of the passage of flux transfer events (Russell & Elphic, 1978). Such excursions are seen in Figure 2, at 0250 UT, at 0251:30 UT (identified by the black arrow in Figure 2c), and between 0252 UT and 0254 UT. These bipolar signatures may indicate the presence of small-scale flux ropes as discussed by Daughton et al. (2011) and Nakamura et al. (2016), but the detailed analysis is beyond the scope of this paper. The time period between 0250 and 0251:30 UT in between the positive/negative B_x excursions is identified by the gray trapezoid in Figure 2a) and is discussed in detail below.

Figure 3 shows the same 20-min interval as in Figure 2. The panels from top to bottom (Figures 3a–3d) are the omnidirectional proton flux, the omnidirectional electron flux, the B_z GSM component of the magnetic field, and the electron fluxes at 800 eV parallel (black traces) and antiparallel (blue traces) to the magnetic field. As in Figure 2, the vertical lines in Figure 3 show the partial and complete crossings of the magnetopause current layer. The electron fluxes parallel and antiparallel to the field are shown in Figure 3d) only in the MSBL/magnetosheath because enhancements in these fluxes have direct and unambiguous bearing on the topology of magnetic field lines in the MSBL. In the LLBL (shaded regions in Figure 3d), the parallel and antiparallel fluxes at 800 eV are nearly equal, which does not provide any unique information on the topology of the field lines (Fuselier et al., 1997).

In the MSBL/magnetosheath, there are time intervals when the omnidirectional electron fluxes in Figure 3b are enhanced at energies greater than about 100 eV. These intervals coincide with enhanced fluxes of >10-keV protons (Figure 3a) and further distinguish the MSBL from the magnetosheath. In particular, there
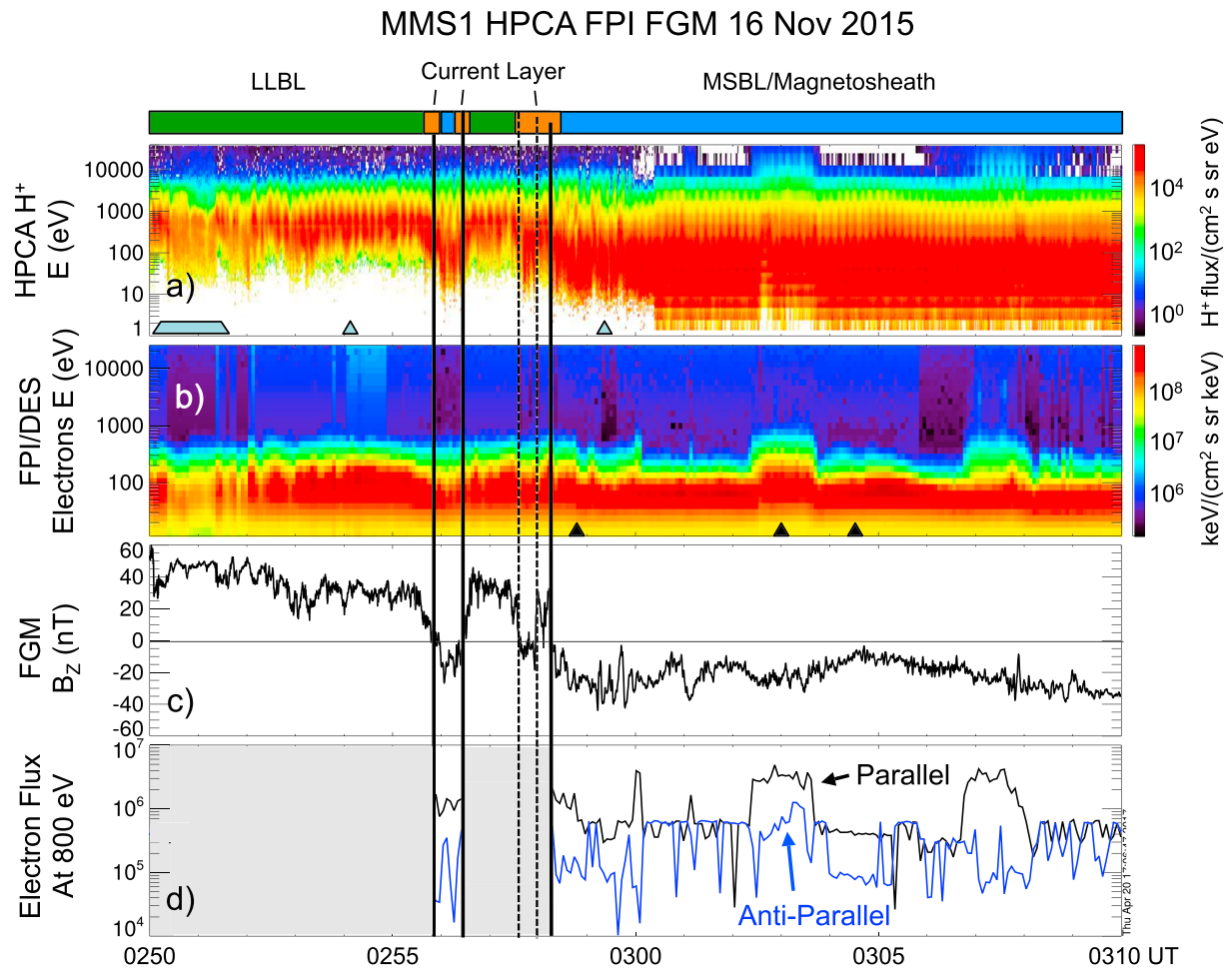
Figure 3. (a) The omnidirectional proton flux, (b) the omnidirectional electron flux, (c) the B_z component, and (d) the parallel and antiparallel electron fluxes at 800 eV for the same magnetopause crossing in Figure 2. In the MSBL, the proton fluxes (a) above 10 keV and the electron fluxes (b) above 100 eV are enhanced over those in the magnetosheath proper. In these MSBL intervals, the 800-eV electrons (d) are often streaming parallel to the magnetic field. For these intervals, there is magnetic connection to a reconnection X line northward of the spacecraft. However, there are a few instances when these electrons in (d) stream both parallel and antiparallel to the field. For these intervals, there is magnetic connection to two X lines northward and southward of the spacecraft. The black triangles in the (b) identify electron energy distributions that are shown in Figure 4.

are streaming energetic protons (>10 keV) and electrons (>200 eV) in the MSBL and the fluxes of energetic protons and electrons are lower in the magnetosheath.

During several of the periods of enhanced energetic protons and electrons, the energetic electrons stream only parallel to the magnetic field. Examples in Figure 3d are the magnetopause crossings from 0255:55 UT to 0256:30 UT, after the last magnetopause crossing at 0258:15 UT, at 0300 UT, and from 0306:30 to 0308 UT. At other times, notably from 0302 to 0303:30 UT in Figure 3d, the energetic electrons stream in both directions along the magnetic field.

To emphasize that the parallel streaming is over a wide range of electron energies, cuts in the electron energy distributions for three different times are shown in Figure 4. Plotted is the electron flux versus energy with negative energies antiparallel to the field and positive energies parallel to the field. The black trace is the electron distribution from 0304:30 UT, when the spacecraft was in the magnetosheath proper. The parallel and antiparallel fluxes are not equal in the magnetosheath because they are not equal in the solar wind (due to the strahl) and there are asymmetries introduced because the two ends of the field lines are connected to two different locations at the bow shock (Feldman et al., 1983). Figure 4a compares this magnetosheath electron distribution with the distribution in the MSBL at 0258:53, just after the final crossing of the magnetopause current layer. The electron energy distributions in the antiparallel direction in the MSBL
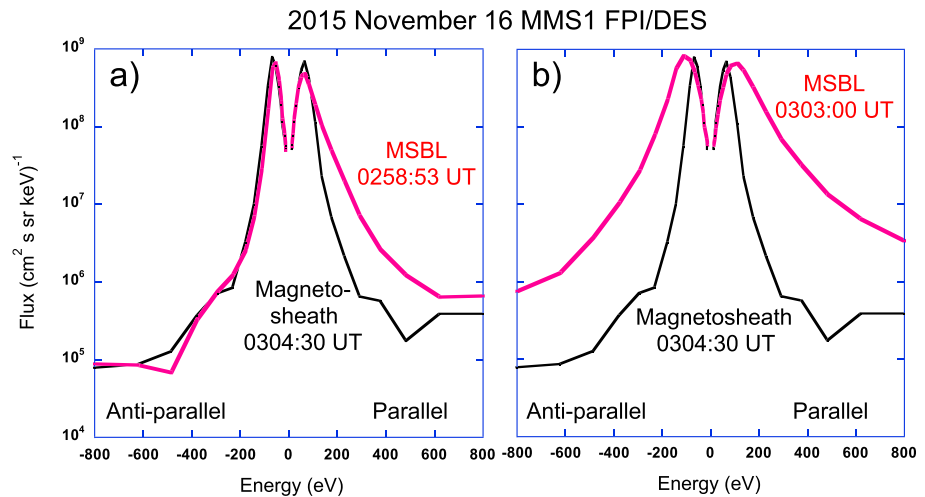
2015 November 16 MMS1 FPI/DES

Figure 4. Flux-energy electron spectrograms comparing the parallel and antiparallel fluxes in the MSBL with those in the magnetosheath. (a) The MSBL at 0258:53 UT is an example of unidirectional, parallel streaming electrons, where the electron fluxes greater than ~100 eV are enhanced compared to the magnetosheath. (b) The MSBL at 0303 UT is an example of bidirectional, parallel and antiparallel streaming electrons, where the electron fluxes greater than ~100 eV are enhanced in both directions along the field compared to the magnetosheath.

and magnetosheath match each other over nearly the entire energy range. However, there is a clear enhancement of electrons in the MSBL that are streaming in the parallel direction. This enhancement extends from ~100 to 800 eV.

Figure 4b compares the magnetosheath electron distribution with the MSBL distribution at 0303 UT, when bidirectional streaming electrons were observed. In this comparison, there are enhanced, streaming electrons both parallel and antiparallel to the magnetic field at energies from ~100 to >800 eV. Electron spectra from other MSBL intervals are similar to the two examples in Figure 4.

Parallel streaming energetic electrons in the MSBL indicate that there is an X line north of the MMS1 spacecraft. From these electron observations alone, the distance to the X line is not known, only its direction relative to the spacecraft. Bidirectional streaming energetic electrons indicate that the spacecraft is between two X lines, one to the north and the other to the south. Again, the distances to the X lines are not known and electrons propagate too fast along the field lines to be able to look at differences in the electron distributions at the different MMS spacecraft.

Summarizing Figures 3 and 4, the MSBL observations indicate that the spacecraft is on reconnected field lines that thread a reconnection site northward of the spacecraft and, occasionally, between two reconnection X lines. Notably, when the spacecraft initially crosses the magnetopause current layers at 0255:55 UT, 0256:30 UT, 0256 UT, and 0258:15 UT, the parallel streaming electrons in Figure 3d are evidence of a single reconnection X line northward of the spacecraft. It is only briefly at 0255:10 UT and later, when the spacecraft returns to the MSBL at 0302 UT that there is evidence of two X lines.

Figure 5 shows two proton velocity space distributions in the LLBL (left panels) and MSBL (right panels), respectively. These two 10-s distributions are identified by the gray triangles in the top panel of Figure 3 and were chosen from several similar distributions to represent the distributions observed in the boundary layers just before and after the magnetopause current layer crossings. The format is the same for both distributions. The top panel shows a 2-D cut in $V_{||}$, $V_\perp$ plane in the frame of reference where the perpendicular bulk velocity of the protons is zero. The bottom panel shows a cut along the $V_{||}$ direction (at $V_\perp = 0$).

The LLBL distribution shows a high-speed proton population propagating at approximately −300 km/s, that is, antiparallel to the magnetic field. Although not apparent in the parallel cut in the bottom panel, there is a second, relatively cold, slower population of magnetospheric protons near-zero parallel velocity. There is also a parallel propagating proton population that looks asymmetric relative to the field direction. This asymmetry is indicative of time aliasing over the 10-s HPCA measurement. The higher-speed, antiparallel
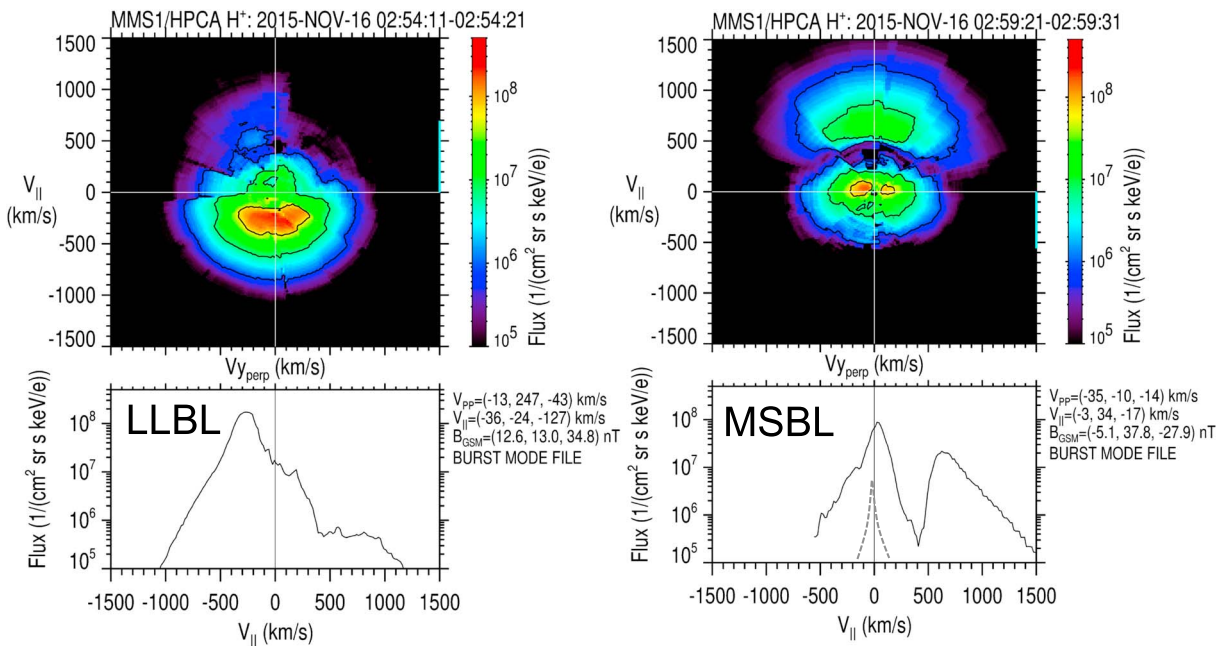
Figure 5. The 2-D and 1-D cuts of 3-D distributions in the (left) LLBL and (right) MSBL from the magnetopause crossing in Figures 2 and 3. The distributions are in the frame of reference where the bulk velocity perpendicular to the magnetic field is zero. The vector velocity transformation is shown next to the 1-D cut and in the 1-D cut in the MSBL, and the dashed curves show the approximate one-count level for the lowest energies. In the left panels, the population streaming antiparallel to the magnetic field at −300 km/s consists of magnetosheath protons from a reconnection X line northward of the spacecraft. At lower parallel velocities, there is a cold magnetospheric proton population. In the right panels, the magnetosheath population is at near-zero parallel velocity and the reflected proton population is at high parallel velocity. The curvature in the low-speed cutoff of reflected proton population indicates that these protons reflected off the magnetopause at a reconnection X line far from the spacecraft.

propagating population consists of magnetosheath protons that entered the LLBL on reconnected field lines. Since the magnetic field is northward in the LLBL, these magnetosheath protons are propagating away from a reconnection X line northward (and dawnward) of the spacecraft. The distribution is curved in the perpendicular direction because it is propagating from a fairly distant location where the magnetic field magnitude is smaller than the magnitude at the spacecraft location. The curvature is not as apparent in the LLBL distribution because of the presence of the cold, lower velocity magnetospheric proton population.

The MSBL distribution in Figure 5 has two proton populations. The first is the magnetosheath population that is at a bulk speed parallel to the field of nearly zero at the subsolar point. The second population is propagating at a bulk speed of +600 km/s, parallel to the magnetic field in the MSBL. This high-speed population consists of magnetosheath protons that have reflected off the magnetopause and, at very high velocities, magnetospheric protons that have crossed the open magnetopause into the MSBL (e.g., Fuselier et al., 1991). Since the magnetic field is southward and duskward in the MSBL, the high-speed population is propagating away from the reconnection X line located northward and dawnward of the spacecraft. The low-speed cutoff of this distribution is also curved in the perpendicular direction because the ions are propagating from a distant region where the magnetic field is weaker than at the subsolar magnetopause. Without a magnetospheric population to mask this population, the curvature in the perpendicular direction is more apparent.

Summarizing Figure 5, the distributions representative of the LLBL and MSBL near the magnetopause crossings each have two proton populations. For the LLBL, one population, propagating antiparallel to the magnetospheric magnetic field at a fairly high speed, is the magnetosheath protons entering from a distant reconnection X line. The second population at near-zero velocity is the cold magnetospheric protons. For the MSBL, one population at near-zero parallel velocity is the magnetosheath population and the other population, propagating at high-speed parallel to the magnetosheath field, is a combination of reflected magnetosheath protons and magnetospheric protons transmitted through the open magnetopause. In
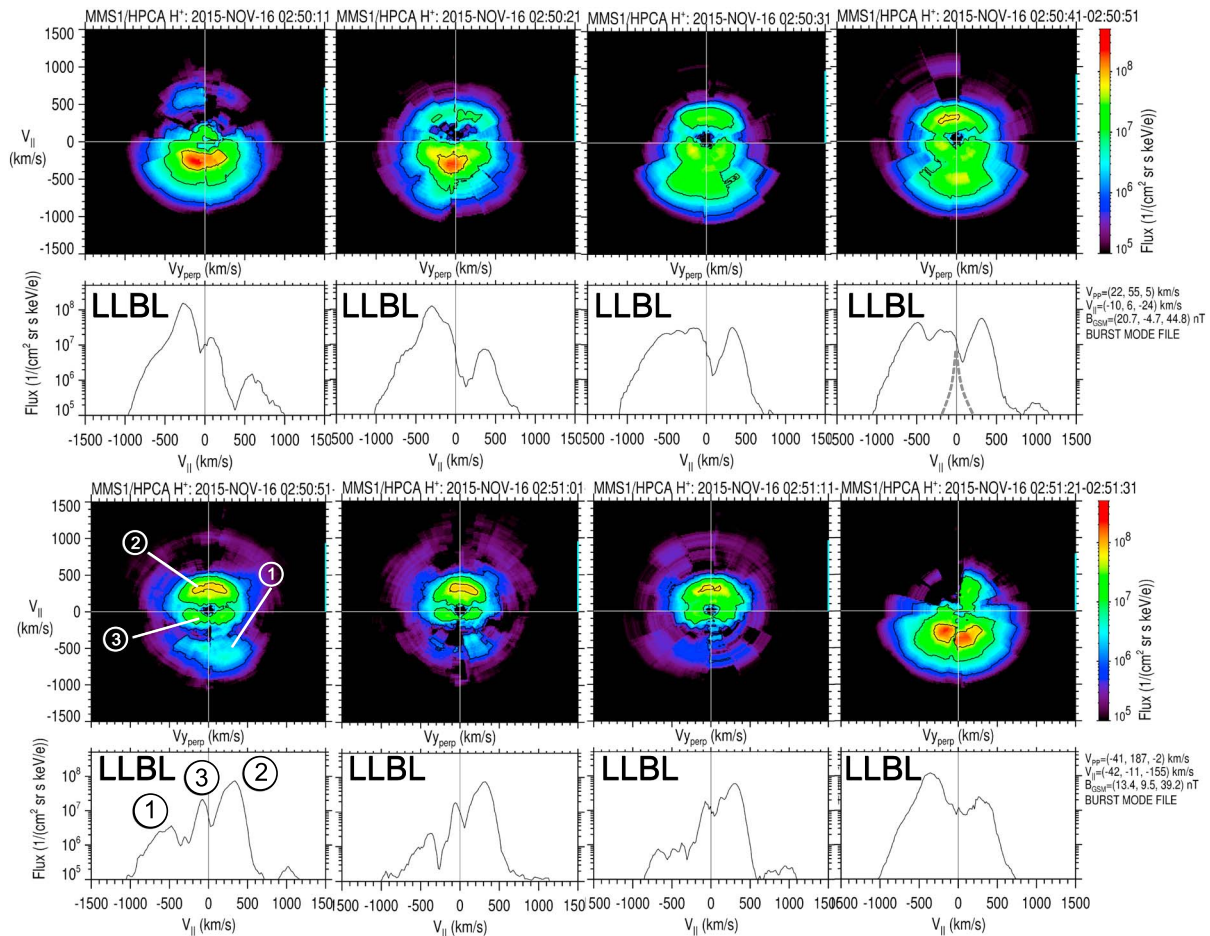
Figure 6. The 2-D and 1-D cuts of 3-D distributions for a LLBL interval shown by the gray trapezoid in Figures 2 and 3. The dashed curves in the 1-D cut for the distribution in the top right shows the approximate one-count level at the lowest energies. All distributions have three proton populations. Population 1 is from the distant reconnection X line northward of the spacecraft. Population 2 is from the close reconnection X line southward of the spacecraft. Population 3 is the cold magnetospheric proton ring beam population. Through the interval, the flux and antiparallel speed of population 1 decreases and then increases while the flux and parallel speed of population 2 does the opposite.

both the LLBL and MSBL in the vicinity of the magnetopause crossings (from 0256 to 0258:15 UT), the high-speed populations are propagating away from a single X line located far from the spacecraft in the northward and dawnward direction.

With the exception of the bidirectional streaming energetic electrons in the MSBL, the observations in Figures 2–5 show that the spacecraft crossed a magnetopause where reconnection was occurring at a fairly distant X line located northward and dawnward of the spacecraft. However, the LLBL interval from 0250 UT to 0251:20 UT (the gray trapezoids in Figures 2 and 3) has a different magnetic field topology. Figure 6 shows the proton distributions through this LLBL interval. Time runs from left to right and top to bottom. To some extent, all the distributions have three proton populations, numbered in the distribution in the bottom left-hand panel in Figure 6. Population 1 is propagating antiparallel to the magnetic field. At the beginning and end of the interval (top leftmost panel and the bottom rightmost panel, respectively), this population has the highest peak flux of the three populations. However, through the interval, the peak flux decreases progressively as the magnitude of its bulk velocity increases. For example, the peak flux for population 1 in the distribution in the bottom left-hand panel is more than an order of magnitude less than its peak flux at the beginning of the interval and the magnitude of the bulk velocity of the population has increased from −250 to −500 km/s. As a point of reference, in this interval, the average local Alfvén speed for 0250–0251:31 UT is ~500 km/s. At the end of the interval, the peak flux of population 1 abruptly increases back to near the original intensity at the beginning of the interval.
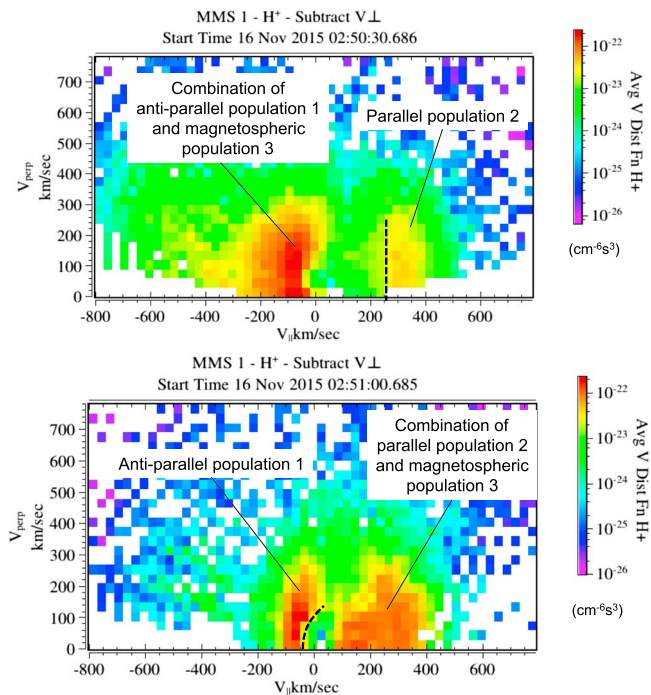
MMS 1 - H⁺ - Subtract V⊥
Start Time 16 Nov 2015 02:50:30.686

MMS 1 - H⁺ - Subtract V⊥
Start Time 16 Nov 2015 02:51:00.685

Figure 7. Proton pitch angle distributions for two selected times in Figure 5. These pitch angle distributions are in the same frame of reference as in Figures 4 and 5. The distributions are created by summing over the pitch angles of the 3-D distribution in this frame of reference. (top) The antiparallel propagating population 1 overlaps with the magnetospheric population 3. The low-speed cutoff of the parallel propagating population 2 (dashed line) is a straight line, indicating that these protons crossed the magnetopause at an X line that was near the spacecraft. (bottom) The parallel propagating population 2 overlaps with the magnetospheric population. The low-speed cutoff of the antiparallel propagating population 1 (dashed curve) is curved, indicating that these protons crossed at an X line that was far from the spacecraft.

At the same time that population 1 is undergoing these changes, population 2, propagating parallel to the field, is doing the opposite. Its peak flux steadily increases until it is dominant and then abruptly decreases at the end of the interval. Also, the magnitude of its bulk velocity steadily decreases from 550 km/s at the beginning of the interval to 300 km/s near the middle and end of the interval.

Population 3 is the magnetospheric ion population. The magnetospheric origin of this population is confirmed from composition measurements (not shown). Previous studies of the magnetospheric population showed that, as it crosses the separatrix from the magnetosphere into the LLBL, it changes character. In particular, in the magnetosphere it appears as a single, cold population. However, in the LLBL, it appears as a double-lobe structure in 2-D cuts and is therefore a ring beam in 3-D (see Vines, Fuselier, Trattner, et al., 2017). The ring beam in Figure 6 has a low, but variable parallel velocity.

The ring beam in Figure 6 is apparent in the top right-hand distribution. This ring beam tends to obscure the low-speed cutoff velocities of populations 2 or 3, depending on the parallel velocity of the beam. The shapes of these low-speed cutoffs are important for determining qualitatively and quantitatively how far the reconnection sites are from the spacecraft (Broll et al., 2017). To emphasize these low-speed cutoffs, Figure 7 shows pitch angle distributions in the frame of reference where $V_\perp = 0$ for two time periods from the interval in Figure 6. These two time periods were selected because the magnetospheric ion population partially overlapped population 1 (top panel) and population 2 (bottom panel).

For the distribution in the top panel of Figure 7, there is no interference between the magnetospheric population at approximately −100-km/s parallel velocity and population 2 at +300 km/s. The low-speed cutoff of population 2 is identified by the dashed line and is a straight line in the perpendicular direction. Given the spacecraft location at a local maximum in the magnetospheric magnetic field, the straight line indicates that this population entered the LLBL from a reconnection site very close to the spacecraft.

Similarly, for the bottom panel of Figure 7, there is no interference between the magnetospheric population at approximately +100-km/s parallel velocity and population 1 at −150 km/s. The low-speed cutoff of population 1 is identified by the dashed curve that follows the low-speed edge of the red colored pixels in the perpendicular direction. The curve indicates that this population entered the LLBL from a reconnection site far from the spacecraft.

Using the procedure outlined in Broll et al. (2017), the distances to the reconnection sites were determined from the degree of curvature of the low-speed cutoffs of populations 1 and 2. Population 1, with large curvature, crossed the magnetopause northward and dawnward and at least 4 R_E from the spacecraft. In contrast, population 2, with little or no curvature, crossed the magnetopause southward and duskward at 1 R_E or less from the spacecraft. The uncertainty in these distances is of the order of 1 R_E.

4. Discussion

Figure 8 is a schematic of the reconnection structure encountered by the MMS spacecraft on 16 November 2015. The right-hand side shows a 2-D projection onto the Y_{GSM}-Z_{GSM} plane of the magnetic shear angles at the magnetopause. High shear angles are red and low shear angles are violet. The circle is the terminator and, according to the maximum shear model (Trattner et al., 2007), the primary X line stretches from the dawn flank to dusk flank. On the dawn and dusk flanks, this X line follows the high-shear, antiparallel reconnection region. However, on the dawnside, the reconnection line deviates from the antiparallel location and
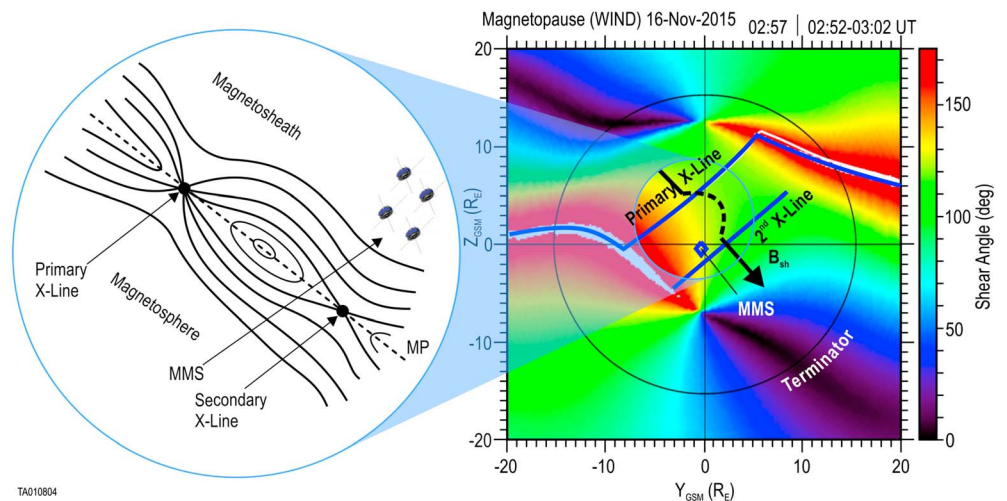
Figure 8. Schematic of the multiple X line structure encountered by the MMS spacecraft on 16 November 2015. The spacecraft crossed the magnetopause at the subsolar point. The crossing occurred approximately 4 R_E southward of a quasi-stationary primary X line and approximately 1 R_E northward of a quasi-stationary secondary X line. The maximum shear model predicts that the primary X line is long and continuous and extends from the antiparallel reconnection region on the dawn flank through a component reconnection X line that connects to the antiparallel reconnection region on the dusk flank. The secondary X line is either intermittent in time or does not reconnect all of the magnetic flux that is reconnected at the primary X line.

cuts across the dayside magnetopause. The X line crosses the noon meridian at fairly high latitude and connects to the antiparallel reconnection region on the duskside.

The electron observations in Figures 3b, 3d, and 4 and the proton observations in Figures 2a, 5, and 6 were used to guide the schematic cross section of the magnetopause in the left-hand panel of Figure 8. These combined observations indicate that the MMS spacecraft crossed the magnetopause approximately 4 R_E from a quasi-stationary primary X line. As the spacecraft transitioned into the MSBL and for most of the LLBL, MMS1 was on field lines that were connected only to this relatively distant X line. However, some of the time in the MSBL and LLBL, the spacecraft was on field lines that were connected to a quasi-stationary secondary X line that was within 1 R_E of the spacecraft. The relative spacing in Figure 8 is not to scale. In reality, the MSBL and LLBL are much thinner than the separation of the primary and secondary X lines and the MMS spacecraft were approximately 10 km apart. With these close spacecraft separations, the HPCAs observed no difference in the ion distributions among the four spacecraft.

The primary X line is located where the maximum shear model predicts an X line. Therefore, the X line forms there probably because that is the region between the two antiparallel locations where the shear is highest along a single, continuous line. The secondary X line is located near the subsolar point. This location may be the result of reconnection that is initiated at the first location where the magnetosheath field line impacts the magnetopause; however, this is only a suggestion.

The primary/secondary X line structure in Figure 8 is quasi-stationary. Over the 1.5 min that the primary/secondary X line structure is observed, the low-speed cutoff of the parallel propagating population from the secondary X line is a straight line, indicating that these protons crossed the magnetopause at an X line that was near the spacecraft. In contrast, over the 1.5 min, the low-speed cutoff of the antiparallel propagating population from the primary X line is curved, indicating that these protons crossed at an X line that was far from the spacecraft. In the MSBL (Figure 5), the low-speed cutoff of the population from the primary X line (the antiparallel propagating population in this case) is also curved, indicating that the primary X line did not move over many minutes. If the primary X line were propagating at several hundreds of kilometers per second, as some simulations show (Hoilijoki et al., 2017; Raeder, 2006), then it would pass completely over the spacecraft in 1.5 min. Even if it were propagating at ~100 km/s, the primary X line would reach the spacecraft in 4 min and there would be evidence of motion in the 1.5 min of observation.

This stationarity is in contrast to a flux transfer event and to simulations of multiple X lines. An FTE propagates along the magnetopause and, if it is bounded by two X lines, then the two X lines also propagate along the boundary. That is not to say that there are no FTE-like signatures in the observations. In particular, Figure 2 shows that there are two positive/negative excursions in the B_x component (on much smaller time scales) at the beginning and end of the interval in Figure 6. As discussed in the previous section, these bipolar signatures may indicate the presence of small-scale flux transfer events identified in simulations by Daughton et al. (2011) and Nakamura et al. (2016), but the detailed analysis is beyond the scope of this paper. These excursions are FTE-like, but the entire 1.5-min interval does not have large-scale FTE-like signatures in the magnetic field. Similarly, the simulations show motion of both X lines. It is true that the motion is neither constant nor in one direction. However, the X lines move (Chen et al., 2017; Hoilijoki et al., 2017).

Although the primary and secondary X lines are quasi-stationary, it is not clear from the observations if the secondary X line is intermittent (i.e., it disappears and reforms over the course of the ~20-min interval in Figure 3). This X line is only observed during a small part of the total LLBL and MSBL time intervals. There are two diametrically opposed interpretations of these intermittent observations. Either the reconnection X line is transient in time, or as depicted in Figure 8, not all of the magnetic field lines that reconnect at the primary line also reconnect at the secondary line. The spacecraft are too close together and the thicknesses of the layers and sizes of the structures are too large to use individual spacecraft observations to separate time and space and distinguish these two interpretations. Also, burst data are not available for the entire interval, requiring the use of lower time resolution (4.5 s) data for the electron parallel/antiparallel fluxes. Therefore, it is not possible to use the electron fluxes from the individual spacecraft as an independent measure of the distance to the reconnection X lines.

Finally, Figure 8 depicts quasi-two-dimensional reconnection X line structures. There is evidence in the observations that the large magnetic "island" in Figure 8 has a more flux rope-like, 3-D structure. In Figure 6, the low-speed cutoff velocities of populations 1 and 2 change in a systematic way. As the low-speed cutoff velocity of population 1 decreases, the low-speed cutoff velocity of population 2 increases. In a purely 2-D geometry as depicted in Figure 8, these systematic changes in the two cutoff velocities are not possible. In a 2-D geometry, the low-speed cutoff velocity decreases as the spacecraft moves closer to the magnetopause, regardless of the distance or direction to the reconnection site or sites. Therefore, the increase in the low-speed cutoff velocity of one population and the simultaneous decrease in the velocity for another population indicate that there is 3-D structure to the large-scale magnetic island in Figure 8. In other words, the island is likely a large-scale flux rope with twisted magnetic fields. Typically, flux rope structures have twisted magnetic fields and distinct field orientation signatures. However, the island structure could be quite large and not all field lines are connected to both reconnection X lines. These complications create problems for using, for example, the normal component of the magnetic field at the magnetopause as a guide to the internal structure.

Table 1 lists nine magnetopause crossings, including the one featured in Figures 1–8, where the MMS spacecraft were located near the subsolar region and IMF conditions were similar to those in Figure 1. These magnetopause crossings were identified starting with a list of magnetopause crossings within a few R_E of the subsolar point from 2015 to 2016 (MMS phase 1a). The spacecraft were near the subsolar point on the outbound leg of their orbits from 1 November to about 1 December 2015. Then they were near the subsolar point on the inbound leg of their orbits from 1 December to 31 December 2015. Since the orbit period is nearly 1 day, there were approximately 60 magnetopause crossings in the initial list. The following two additional criteria were imposed: (1) $|B_x|/B < 0.7$, to reduce the difficulty for the magnetic shear mapping at the magnetopause, and (2) $| \pm B_y| > |-B_z|$ for at least a few minutes surrounding the magnetopause crossing. Nine of the initial approximately 60 magnetopause crossings met all of these criteria. The clock angles for these nine events are listed in column 3. By design, they are all between either 90° and 135° or 225° and 270°. That is, they are all events when the IMF was southward with an IMF B_y component that was greater than or equal to the $|B_z|$ component. The spacecraft location and the criterion on the IMF components were used to reproduce the conditions in Figure 8. Under these conditions, the spacecraft is near the subsolar point and the prime reconnection line, as predicted by the maximum magnetic shear model, is many R_E from the spacecraft.

Table 1
Observations of Bidirectional Streaming Energetic Electrons in the MSBL and Multiple Counterstreaming Ion Populations in the LLBL That Indicate Large-Scale Multiple Reconnection at the Magnetopause

Date	Magnetopause Time	Clock Angle (deg, With 0° Defined Along +Z_{GSM})	Bidirectional Streaming Electrons in the MSBL (Y or N)	Multiple Counterstreaming Ion Populations in the LLBL (Y or N)	Solar Wind Dynamic Pressure Convected to the Magnetopause
1 November 2015	0338:00 UT	112	Y	Y	2.2
14 November 2015	0317:30 UT	111	Y	Y	1.7
16 November 2015	0258:10 UT	129	Y	Y	1.3
1 December 2015	0136:40 UT	262	Y	N	2.1
2 December 2015	0812:10 UT	117	N	N	0.9
9 December 2015	1112:40 UT	126	Y	Y?	1.8
13 December 2015	0931:40 UT	122	Y	Y	1.7
21 December 2015	1033:10 UT	249	Y?	Y	1.5
22 December 2015	1130:30 UT	225	N	N	2.1

Note. The question marks beside the Y or N indicate that there is some uncertainty in the interpretation.

The boundary layers associated with these crossings were investigated for evidence of large-scale, multiple reconnection X lines at the magnetopause. This evidence includes bidirectional streaming heated electrons in the MSBL as in Figures 3 and 4 at 0303 UT and/or multiple, counterstreaming ion populations in the LLBL as in Figure 6. Only two of the nine crossings did not display any evidence for multiple reconnection X lines during the encounters with the boundary layers. The rest had one or the other or both pieces of evidence.

If the secondary X line is formed in the subsolar region because that is where the magnetosheath field line first encounters the magnetopause, then it is possible that higher solar wind dynamic pressures could facilitate this formation. The last column in Table 1 shows the solar wind dynamic pressure convected to the magnetopause for the nine magnetopause crossings. Although the numbers are small, there is no apparent correlation between evidence of multiple reconnection X lines and higher solar wind dynamic pressure. Most of the solar wind dynamic pressures are nominal. Although it is true that the lowest pressure is associated with one of the crossings that did not display any evidence for multiple X lines, the other crossing that showed no evidence had one of the higher solar wind dynamic pressures of the group.

Table 1 should not be considered a survey of large-scale multiple X line reconnection evidence. Such a survey would require determining the total length of time that the spacecraft location and IMF conditions were similar to those for the 16 November 2015 magnetopause crossing. Further, such a survey would require some sort of quantitative measure of the probability of detecting evidence for multiple reconnection X lines. Finally, a survey would require many more events by relaxing the restrictive criteria on the spacecraft location and the IMF components that was used to identify the nine events in Table 1. From Figures 3 and 6, it is clear that bidirectional streaming electrons and counterstreaming ion populations are observed only part of the time that the spacecraft are in the boundary layers. For example, the spacecraft remained in the LLBL and MSBL for many minutes for the crossing on 16 November 2015. For typical crossings the spacecraft are in the boundary layers, especially the MSBL, for much shorter time. Thus, evidence for large-scale, multiple reconnection could be missed by HPCA observations for more rapid magnetopause crossings. Although not a survey, Table 1 should be taken as evidence that large-scale, multiple reconnection X lines may be common at the dayside magnetopause under the specific range of conditions in Figure 8 and Table 1.

References

Broll, J. M., Fuselier, S. A., & Trattner, K. J. (2017). Locating dayside magnetopause reconnection with exhaust ion distributions. *Journal of Geophysical Research: Space Physics*, *122*, 5105–5113. https://doi.org/10.1002/2016JA023590

Burch, J. L., Moore, T. E., Torbert, R. B., & Giles, B. L. (2016). Magnetospheric Multiscale overview and science objectives. *Space Science Reviews*, *199*(1-4), 5–21. https://doi.org/10.1007/s11214-015-0164-9

Chen, Y., Toth, G., Cassak, P., Jia, X., Gombosi, T. I., Slavin, J. A., et al. (2017). Global three-dimensional simulation of Earth's dayside reconnection using a two-way coupled magnetohydrodynamics with embedded particle-in-cell model: Initial results. *Journal of Geophysical Research: Space Physics*, *122*, 10,318–10,335. https://doi.org/10.1002/2017JA024186

Cowley, S. W. H. (1982). The causes of convection in the Earth's magnetosphere: A review of developments during the IMS. *Reviews of Geophysics and Space Physics*, *20*(3), 531–565. https://doi.org/10.1029/RG020i003p00531

Daughton, W., Roytershteyn, V., Karimabadi, H., Yin, L., Albright, B. J., Bergen, B., & et al. (2011). Role of electron physics in the development of turbulent magnetic reconnection in collisionless plasmas. *Nature Physics*, *7*(7), 539–542. https://doi.org/10.1038/NPHYS1965

Drake, J. F., Swisdak, M., Che, H., & Shay, M. A. (2006). Electron acceleration from contracting magnetic islands during reconnection. *Nature*, *443*(7111), 553–556. https://doi.org/10.1038/nature05116

Drake, J. F., Swisdak, M., Schoeffler, K. M., Rogers, B. N., & Kobayashi, S. (2006). Formation of secondary islands during magnetic reconnection. *Geophysical Research Letters*, *33*, L13105. https://doi.org/10.1029/2006GL025957

Dunlop, M. W., Zhang, Q. H., Bogdanova, Y. V., Trattner, K. J., Pu, Z., Hasegawa, H., et al. (2011). Magnetopause reconnection across wide local time. *Annales de Geophysique*, *29*(9), 1683–1697. https://doi.org/10.5194/angeo-29-1683-2011

Eastwood, J. P., Phan, T. D., Cassak, P. A., Gershman, D. J., Haggerty, C., Malakit, K., et al. (2016). Ion-scale secondary flux ropes generated by magnetopause reconnection as resolved by MMS. *Geophysical Research Letters*, *43*, 4716–4724. https://doi.org/10.1002/2016GL068747

Feldman, W. C., Anderson, R. C., Bame, S. J., Gary, S. P., Gosling, J. T., McComas, D. J., et al. (1983). Electron velocity distributions near the Earth's bow shock. *Journal of Geophysical Research*, *88*(A1), 96–110. https://doi.org/10.1029/JA088iA01p00096

Fuselier, S. A., Anderson, B. J., & Onsager, T. G. (1995). Particle signatures of magnetic topology at the magnetopause: AMPTE/CCE observations. *Journal of Geophysical Research*, *100*(A7), 11,805–11,822. https://doi.org/10.1029/94JA02811

Fuselier, S. A., Anderson, B. J., & Onsager, T. G. (1997). Electron and ion signatures of field line topology at the low shear magnetopause. *Journal of Geophysical Research*, *102*(A3), 4847–4863. https://doi.org/10.1029/96JA03635

Fuselier, S. A., Frey, H. U., Trattner, K. J., Mende, S. B., & Burch, J. L. (2002). Cusp aurora dependence on interplanetary magnetic field B_z. *Journal of Geophysical Research*, *107*(A7), 1111. https://doi.org/10.1029/2001JA900165

Fuselier, S. A., Klumpar, D. M., & Shelley, E. G. (1991). Ion reflection and transmission during reconnection at the Earth's subsolar magnetopause. *Geophysical Research Letters*, *18*(2), 139–142. https://doi.org/10.1029/90GL02676

Fuselier, S. A., Lewis, W. S., Schiff, C., Ergun, R., Burch, J. L., Petrinec, S. M., & et al. (2016). Magnetospheric Multiscale science mission profile and operations. *Space Science Reviews*, *199*(1-4), 77–103.

Fuselier, S. A., Petrinec, S. M., Trattner, K. J., & Lavraud, B. (2014). Magnetic field topology for northward IMF reconnection: Ion observations. *Journal of Geophysical Research: Space Physics*, *119*, https://doi.org/10.1002/2014JA020351, 9051–9071.

Fuselier, S. A., Trattner, K. J., & Petrinec, S. M. (2011). Antiparallel and component reconnection at the dayside magnetopause. *Journal of Geophysical Research*, *116*, A10227. https://doi.org/10.1029/2011JA016888

Fuselier, S. A., Trattner, K. J., Petrinec, S. M., & Lavraud, B. (2012). Dayside magnetic topology at the Earth's magnetopause for northward IMF. *Journal of Geophysical Research*, *117*, A08235. https://doi.org/10.1029/2012JA017852

Hasegawa, H., Wang, J., Dunlop, M. W., Pu, Z. Y., Zhang, Q. H., Lavraud, B., et al. (2010). Evidence for a flux transfer event generated by multiple X-line reconnection at the magnetopause. *Geophysical Research Letters*, *37*, L16101. https://doi.org/10.1029/2010GL044219

Hoilijoki, S., Ganse, U., Pfau-Kempf, Y., Cassak, P. A., Walsh, B. M., Hietala, H., et al. (2017). Reconnection rates and X line motion at the magnetopause: Global 2D-3V hybrid-Vlasov simulation results. *Journal of Geophysical Research: Space Physics*, *122*, 2877–2888. https://doi.org/10.1002/2016JA023709

Kacem, I., Jacquey, C., Génot, V., Lavraud, B., Vernisse, Y., Marchaudon, A., et al. (2018). Magnetic reconnection at a thin current sheet separating two interlaced flux tubes at the Earth's magnetopause. *Journal of Geophysical Research: Space Physics*, *123*, 1779–1793. https://doi.org/10.1002/2017JA024537

Lavraud, B., Thomsen, M. F., Lefebvre, B., Schwartz, S. J., Seki, K., Phan, T. D., et al. (2006). Evidence for newly closed magnetosheath field lines at the dayside magnetopause under northward IMF. *Journal of Geophysical Research*, *11*, A05211. https://doi.org/10.1029/2005JA011266

Lavraud, B., Thomsen, M. F., Taylor, M. G. G. T., Wang, Y. L., Phan, T. D., Schwartz, S. J., et al. (2005). Characteristics of the magnetosheath electron boundary layer under northward interplanetary magnetic field: Implications for high-latitude reconnection. *Journal of Geophysical Research*, *110*, A06209. https://doi.org/10.1029/2004JA010808

Lee, L. C., & Fu, Z. F. (1986). Multiple X line reconnection. I. A criterion for the transition from a single X line to multiple X line reconnection. *Journal of Geophysical Research*, *91*(A6), 6807. https://doi.org/10.1029/JA091iA06p06807

Lepping, R. P., Acuna, M. H., Burlaga, L. F., Farrell, W. M., Slavin, J. A., Schatten, K. H., et al. (1995). The wind magnetic field instrument. In C. T. Russell (Ed.), *The Global Geospace Mission*, (pp. 207–229). The Netherlands: Kluwer Academic Press.

Nakamura, T. K. M., Nakamura, R., Narita, Y., Baumjohann, W., & Daughton, W. (2016). Multi-scale structures of turbulent magnetic reconnection. *Physics of Plasmas*, *23*(5), 052116. https://doi.org/10.1063/1.4951025

Ogilvie, K. W., Chornay, D. J., Fitzenreiter, R. J., Hunsaker, F., Keller, J., Lobell, J., et al. (1995). SWE: A comprehensive plasma instrument for the wind spacecraft. In C. T. Russell (Ed.), *The Global Geospace Mission*, (pp. 55–77). Norwell, MA: Kluwer Academic Press.

Øieroset, M., Phan, T. D., Haggerty, C., Shay, M. A., Eastwood, J. P., Gershman, D. J., et al. (2016). MMS observations of large guide field 1 symmetric reconnection between colliding reconnection jets at the center of a magnetic flux rope at the magnetopause. *Geophysical Research Letters*, *43*, 5536–5544. https://doi.org/10.1002/2016GL069166

Owen, C. J., Marchaudon, A., Dunlop, M. W., Fazakerley, A. N., Bosqued, J.-M., Dewhurst, J. P., et al. (2008). Cluster observations of "crater" flux transfer events at the dayside high-latitude magnetopause. *Journal of Geophysical Research*, *113*, A07S04. https://doi.org/10.1029/2007JA012701

Petrinec, S. M., Burch, J. L., Fuselier, S. A., Gomez, R. G., Lewis, W., Trattner, K. J., et al. (2016). Comparison of Magnetospheric Multiscale ion jet signatures with predicted reconnection site locations at the magnetopause. *Geophysical Research Letters*, *43*, 5997–6004. https://doi.org/10.1002/2016GL069626

Petrinec, S. M., Dayeh, M. A., Funsten, H. O., & Fuselier, S. A. (2011). Neutral atom imaging of the magnetospheric cusps. *Journal of Geophysical Research*, *116*, A07203. https://doi.org/10.1029/2010JA016357

Phan, T. D., Kistler, L. M., Klecker, B., Haerendel, G., Paschmann, G., Sonnerup, B. U. Ö., et al. (2000). Extended magnetic reconnection at the Earth's magnetopause from detection of bi-directional jets. *Nature*, *404*(6780), 848–850. https://doi.org/10.1038/35009050

Pollock, C., Moore, T., Jacques, A., Burch, J., Gliese, U., Saito, Y., et al. (2016). Fast plasma investigation for magnetosphere multiscale. *Space Science Reviews*, *199*(1-4), 331–406. https://doi.org/10.1007/s11214-016-0245-4

Raeder, J. (2006). Flux transfer events: 1. Generation mechanism for strong southward IMF. *Annales Geophysicae*, *24*(1), 381–392. https://doi.org/10.5194/angeo-24-381-2006

Russell, C. T., Anderson, B. J., Baumjohann, W., Bromund, K. R., Dearborn, D., Fischer, D., et al. (2016). The Magnetospheric Multiscale magnetometers. *Space Science Reviews*, *199*(1-4), 189–256. https://doi.org/10.1007/s11214-014-0057-3

Russell, C. T., & Elphic, R. C. (1978). Initial ISEE magnetometer results: Magnetopause observations. *Space Science Reviews*, *22*, 681–715.

Russell, C. T., Strangeway, R. J., Zhao, C., Anderson, B. J., Baumjohann, W., Bromund, K. R., et al. (2017). Structure, force balance, and topology of Earth's magnetopause. *Science*, *356*(6341), 960–963. https://doi.org/10.1126/science.aag3112

Scholer, M. (1988). Magnetic flux transfer at the magnetopause base on single X line bursty reconnection. *Geophysical Research Letters*, *15*(4), 291–294. https://doi.org/10.1029/GL015i004p00291

Southwood, D. J., Farrugia, C. J., & Saunders, M. A. (1988). What are flux transfer events? *Planetary and Space Science*, *36*(5), 503–508. https://doi.org/10.1016/0032-0633(88)90109-2

Trattner, K. J., Burch, J. L., Ergun, R., Eriksson, S., Fuselier, S. A., Giles, B. L., et al. (2017). The MMS dayside magnetic reconnection locations during phase 1 and their relation to the predictions of the maximum magnetic shear model. *Journal of Geophysical Research: Space Physics*, *122*, https://doi.org/10.1002/2017JA024488, 11,991–12,005.

Trattner, K. J., Mulcock, J. S., Petrinec, S. M., & Fuselier, S. A. (2007). Location of the reconnection line at the magnetopause during southward IMF conditions. *Geophysical Research Letters*, *34*, L03108. https://doi.org/10.1029/2006GL028397

Trattner, K. J., Petrinec, S. M., Fuselier, S. A., & Phan, T. D. (2012). The location of reconnection at the magnetopause: Testing the maximum shear model with THEMIS observations. *Journal of Geophysical Research*, *117*, A01201. https://doi.org/10.1029/2011JA016959

Tsyganenko, N. A. (2014). Data-based modeling of the geomagnetosphere with an IMF-dependent magnetopause. *Journal of Geophysical Research: Space Physics*, *119*, 335–354. https://doi.org/10.1002/2013JA019346

Vines, S. K., Fuselier, S. A., Petrinec, S. M., Trattner, K. J., & Allen, R. C. (2017). Occurrence frequency and location of magnetic islands at the dayside magnetopause. *Journal of Geophysical Research: Space Physics*, *122*, 4138–4155. https://doi.org/10.1002/2016JA023524

Vines, S. K., Fuselier, S. A., Trattner, K. J., Burch, J. L., Allen, R. C., Petrinec, S. M., et al. (2017). Magnetospheric ion evolution across the low-latitude boundary layer separatrix. *Journal of Geophysical Research: Space Physics*, *122*, 10,247–10,262. https://doi.org/10.1002/2017JA024061

Vines, S. K., Fuselier, S. A., Trattner, K. J., Petrinec, S. M., & Drake, J. F. (2015). Ion acceleration dependence on magnetic shear angle in dayside magnetopause reconnection. *Journal of Geophysical Research: Space Physics*, *120*, 7255–7269. https://doi.org/10.1002/2015JA021464

Young, D. T., Burch, J. L., Gomez, R. G., De Los Santos, A., Miller, G. P., Wilson, P., et al. (2014). Hot plasma composition analyzer for the Magnetospheric Multiscale mission. *Space Science Reviews*, *199*(1-4), 407–470. https://doi.org/10.1007/s11214-014-0049-6